Supplementary Information

ATP binding controls distinct structural transitions of *Escherichia coli* DNA gyrase in complex with DNA

Aakash Basu, Allyn J. Schoeffler, James M. Berger, and Zev Bryant

Table of Contents

SUPPLEMENTARY FIGURES

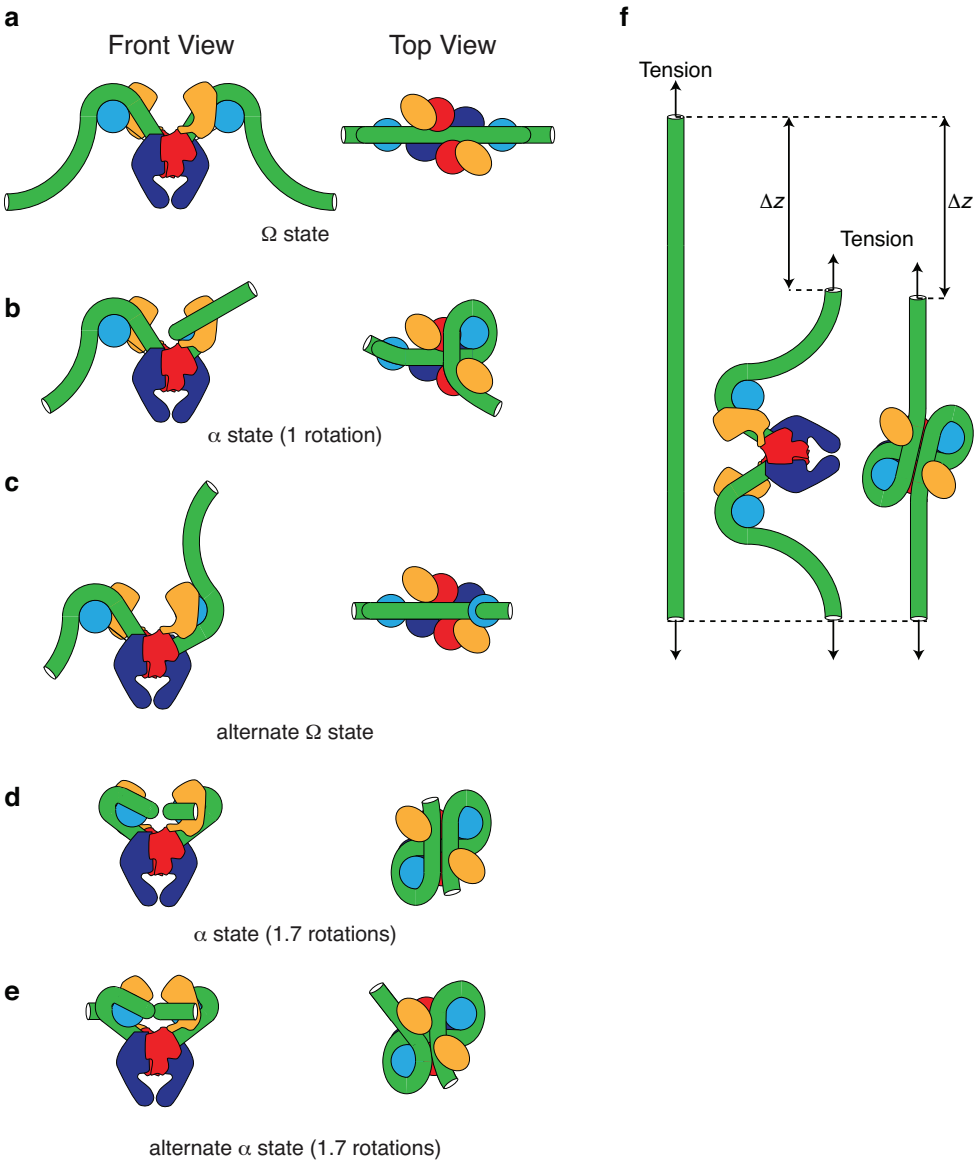

Supplementary Figure 1 Possible geometries of α and Ω states under tension. Speculative illustrations are shown for the Ω state and for α state variants that trap ~1 supercoil or ~1.7 supercoils. Other configurations are possible; for example, since we do not directly observe the placement of CTDs, we cannot rule out alternative arrangements in which the CTDs are near the exit gate[1] in one or both of the Ω and α states. Moreover, states may be flexible; for example, states such as (**a**) and (**c**) may coexist with other configurations in the Ω state to yield writhe that is zero on average. In the ~1.7 rotation variant of the α state, two potential T-segments may be simultaneously docked (**d**) as proposed earlier[2]

for yeast topoisomerase II, or (**e**) one of the potential T-segments may be excluded from the cavity. The ~1 rotation and ~1.7 rotation variants of the α state are structurally distinct but functionally and kinetically indistinguishable in our assays. Panel (**f**) illustrates the conversion of free DNA to the Ω state (shown in front view) with a large contraction in z, followed by conversion from Ω to α without any large change in z. In this speculative diagram, the angle between DNA segments exiting the complex in Ω compensates for exit points that are closer to each other in α.

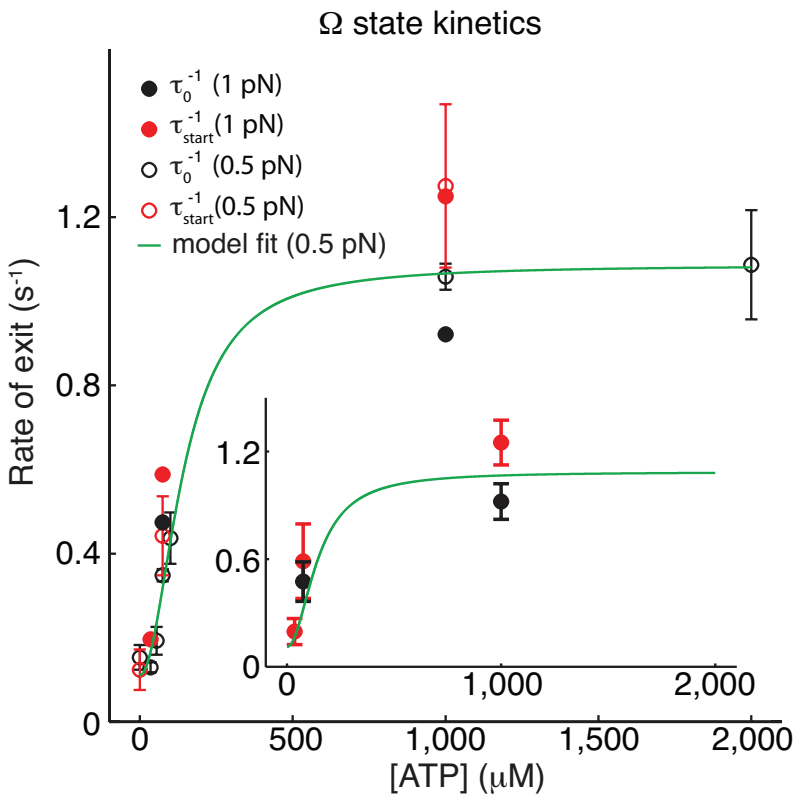

Supplementary Figure 2 Force dependent kinetics of the Ω to α transition. Rates of exit are shown as a function of [ATP] for data taken at 0.5 pN (reproduced from **Fig. 6**) and at 1 pN. Two different measures of Ω state lifetime are plotted: the duration of the dominant pause (τ_0) and also the lag time (τ_{start}) between contraction and rotation at the beginning of a processive burst. Standard errors are shown for 0.5 pN data in the main panel, and for 1 pN data in the inset. We conclude that the rate of the Ω to α transition is not substantially affected by tension in this range.

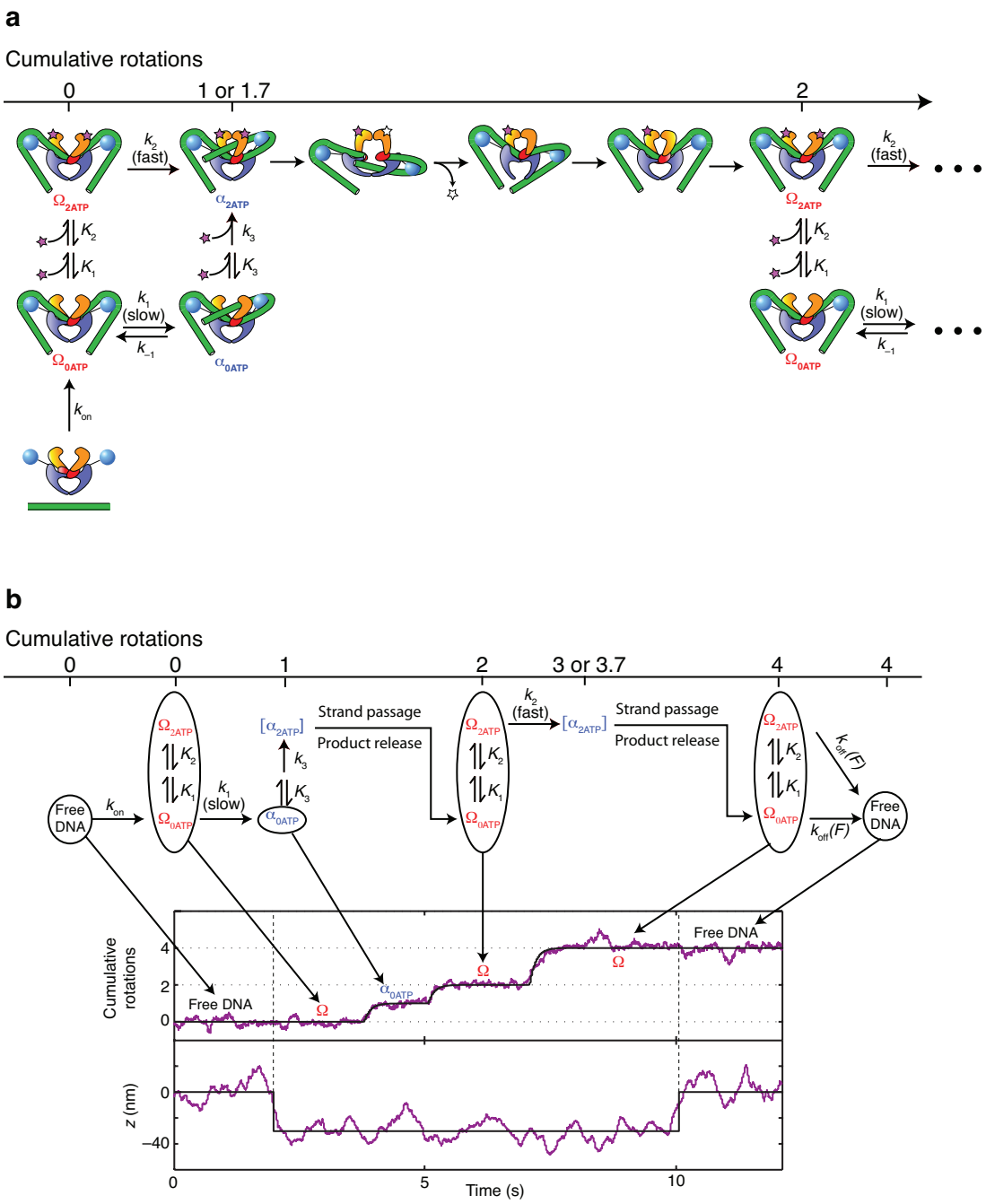

Supplementary Figure 3 Correspondence between angular position of the rotor and states in the mechanochemical cycle. **(a)** The branched kinetic model (**Fig. 7**) is redrawn with states arranged in columns corresponding to rotational positions, and annotated to show the number of rotations of the reporter bead associated with each column. (**b)** A sample rotor bead trace has been annotated to indicate the likely sequence of states visited during this particular burst. Square brackets are used to denote states that are too short-lived to be detected as dwells in the rotor bead trace.

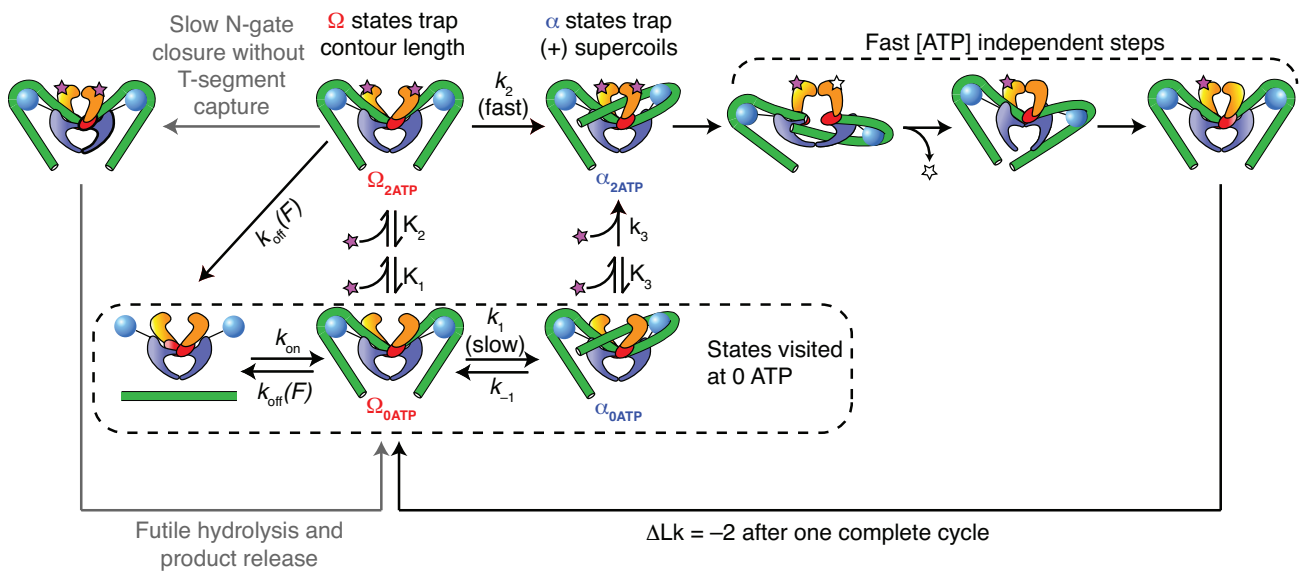

Supplementary Figure 4 Expanded mechanochemical model. The branched kinetic model (**Fig. 7**) is expanded here to show potential unproductive cycles (gray) in which the ATP gate closes without capturing a T-segment, and ATP hydrolysis is required to re-open the gate. We hypothesize that these futile cycles are avoided in DNA gyrase because gate closure in Ω_{2ATP} is slow in comparison to k_2. This contrasts with yeast topoisomerase II, which is thought to perform several futile hydrolysis cycles per strand passage[3] at high [ATP]. At very low [ATP], both enzymes avoid futile cycles because T-segment docking precedes ATP binding — in DNA gyrase, this corresponds to the pathway through α_{0ATP}.

According to our hypothesis, a T-segment is required for rapid nucleotide-driven N-gate closure. In our kinetic model (Figure 7 and above), there are long dwells in Ω with ATP bound to both ATPase domains. The N-gate may remain open during these dwells, if there is a kinetic barrier to closure in the absence of a T-segment. A conformational fluctuation from Ω to α can then be efficiently trapped by rapid nucleotide-driven gate closure triggered by the T-segment. A similar mechanism of ATP conservation has been proposed for the bacterial Hsp90 protein HtpG, in which slow ATP-mediated dimerization is accelerated in the presence of substrate[4].

SUPPLEMENTARY NOTES

Kinetic modeling: Parameters for the branched model (**Fig. 7**) were determined by fitting model predictions to measurements of state lifetimes and transition processivity as a function of [ATP]. The rate of exit from the Ω state $k_\Omega = \langle \tau_0 \rangle^{-1} = \langle \tau_{start} \rangle^{-1}$ was modeled assuming $K_1 >> K_2$, giving $k_\Omega = \frac{k_2[ATP]^2}{[ATP]^2 + K_1K_2} + \frac{k_1K_1K_2}{K_1K_2 + [ATP]^2} + k_{off}$, and fit to measured $\langle \tau_0 \rangle$ (**Fig. 6c**). The rate of exit from the α state $k_\alpha = \langle \tau_1 \rangle^{-1} = \langle \tau_{futile} \rangle^{-1}$ was modeled at low [ATP] assuming $K_3 >> [ATP]$, giving $k_\alpha = k_{-1} + \frac{k_3}{K_3}[ATP]^2$, and fit to the average over all categories of α state lifetimes (**Fig. 6c**). The transition processivity $P_T = 1 - \frac{k_{off}}{k_\Omega}$ (**Fig. 7c**, inset) is related to measurable quantities by $P_T = 1 - \langle n_{fut} + n_{for} \rangle^{-1}$, where n_{fut} and n_{for} are the number of futile excursions and forward steps respectively per processive burst, ignoring binding events for which $n_{fut} + n_{for} = 0$. Overall velocity and processivity were predicted from the model with no further fitting. We define the fraction of Ω to α transitions that occur via the ATP-independent branch, $P_{\alpha_0} = \frac{k_1K_1K_2}{K_1K_2 + [ATP]^2}\left(\frac{k_1K_1K_2}{K_1K_2 + [ATP]^2} + \frac{k_2[ATP]^2}{K_1K_2 + [ATP]^2}\right)^{-1}$, and also the probability that an α_{0ATP} state proceeds to strand transfer rather than futile reversion, $P_f = \frac{k_3[ATP]^2}{k_\alpha K_3}$. Supercoiling velocity (**Fig. 7b**) is then given by $V = \frac{1 - P_{\alpha_0} + P_{\alpha_0}P_f}{k_\Omega^{-1} + P_{\alpha_0}k_\alpha^{-1}}$. Processivity (**Fig. 7c**) is given by $P = \frac{P_T(1 - P_{\alpha_0} + P_{\alpha_0}P_f)}{1 - P_TP_{\alpha_0}(1 - P_f)}$ and can be related to measurements using $P = 1 - \frac{1}{\langle n_{for} \rangle}$, ignoring binding events for which $n_{for} = 0$ as in earlier work[5]. Errors in best fit parameters (**Fig. 7a**) were estimated by parametric bootstrap analysis as

described earlier[6] except in the case of $\sqrt{K_1 K_2}$, for which the error was taken from the covariance matrix of the least squares fit, which produced a larger error estimate than the bootstrap.

REFERENCES

1. Baker, N.M., Weigand, S., Maar-Mathias, S. & Mondragon, A. Solution structures of DNA-bound gyrase. *Nucleic Acids Res* (2010).
2. Trigueros, S., Salceda, J., Bermudez, I., Fernandez, X. & Roca, J. Asymmetric removal of supercoils suggests how topoisomerase II simplifies DNA topology. *Journal of molecular biology* **335**, 723-31 (2004).
3. Lindsley, J.E. & Wang, J.C. On the coupling between ATP usage and DNA transport by yeast DNA topoisomerase II. *The Journal of biological chemistry* **268**, 8096-104 (1993).
4. Street, T.O., Lavery, L.A. & Agard, D.A. Substrate binding drives large-scale conformational changes in the Hsp90 molecular chaperone. *Molecular cell* **42**, 96-105 (2011).
5. Gore, J. et al. Mechanochemical analysis of DNA gyrase using rotor bead tracking. *Nature* **439**, 100-4 (2006).
6. Elting, M.W., Bryant, Z., Liao, J.C. & Spudich, J.A. Detailed tuning of structure and intramolecular communication are dispensable for processive motion of myosin VI. *Biophysical journal* **100**, 430-9 (2011).